A minimal model of the bar-resonator vibroacoustic interaction in mallet percussion instruments

Filipe Soares, Jose Antunes, Vincent Debut

Applied Acoustics 199 (2022) 109049

Contents lists available at ScienceDirect

Applied Acoustics

journal homepage: www.elsevier.com/locate/apacoust

A minimal model of the bar-resonator vibroacoustic interaction in mallet percussion instruments

Filipe Soares [a,*], Jose Antunes [a], Vincent Debut [b]

[a] Instituto Superior Técnico – Centro de Ciências e Tecnologias Nucleares, Lisboa, Portugal
[b] Instituto Politécnico de Castelo Branco – Escola Superior de Artes Aplicadas, Castelo Branco, Portugal

ARTICLE INFO

Article history:
Received 4 February 2022
Received in revised form 23 August 2022
Accepted 22 September 2022

Keywords:
Bar-resonator interaction
Vibro-acoustic coupling
Finite element modelling
Marimba
Vibraphone

ABSTRACT

In some mallet percussion instruments, such as vibraphones and marimbas, tubular acoustic resonators are placed beneath the tuned bars to enhance acoustic radiation at their fundamental frequency. This work deals with the formulation of a minimal physical model describing the vibro-acoustic interaction occurring in these instruments. The fundamental bar mode is modelled as a disk-shaped oscillator and the resonator as a cylindrical acoustic waveguide, described in terms of its acoustic modes. The three-dimensional effects associated with sound radiation and the interaction between the two elements are calculated using a 2-D axisymmetric finite element (FE) model, whose numerical results are then fitted to dimensionless analytical expressions, which encapsulate the complex physics of the vibro-acoustic interaction in a simplified manner. This can pragmatically be used to formulate a lumped-parameter model of the coupled system. Illustrative numerical results are presented and qualitatively validated, demonstrating the ability of the proposed modelling approach to capture the essential features of the coupled dynamics occurring in real instruments.

1. Introduction

Mallet percussion instruments are composed of a series of tuned bars, that radiate sound when struck by a mallet. In most modern instruments, tuning is achieved via an undercut on the bar's cross-section, which typically aims to place the frequencies of the first three vertical-bending modes in harmonic relation. A typical tuning ratio found in traditional marimbas and vibraphones is (1:4:10). Nevertheless, recent years have seen a number of studies [1–4] dealing with the tuning of bars via optimization procedures, that illustrate the viability for heterodox tuning ratios, as well as for the tuning of non-vertical-bending modes (torsional, lateral) in parallel with vertical-bending modes [5,6].

Some mallet percussion instruments, like the marimba or the vibraphone, make use of resonator tubes, that are placed beneath the vibrating bars, to enhance the sound radiation. Generally, the fundamental frequency of each tube is tuned near the frequency of the first vertical-bending mode of the corresponding bar. Experimental reports [7,8] demonstrate that the role of the resonator is to enhance the sound radiation of the bar at its fundamental frequency. This is important because: (1) it is the frequency of the first mode that defines the pitch of the struck bar and (2) in general, this mode radiates approximately as a dipole [8], i.e. a fairly inefficient acoustic radiator, as illustrated in Fig. 1.

Most often, resonators are pipes of uniform cross-section (circular, elliptical, rectangular, etc.) with closed-open boundary conditions. This set-up enables tuned resonators to have relatively small lengths, as the fundamental frequency of a closed-open pipe is approximately half the frequency of an open-open pipe of the same length. The natural frequencies of pipes with closed-open boundaries constitute a series of odd harmonics, i.e. $f_n = f_1\,(1:3:5:7\ldots)$ and, due to the tuning ratios found in common bars (1:4:10), typically only their fundamental acoustic mode has a meaningful interaction with the bar vibration. However, we note the work of Henrique et al. [9,10], that have used optimization techniques to design and build resonators with frequencies tuned to a set of pre-defined targets, such that bars and resonators can have matching modal frequencies.

Perhaps the first elucidative study on the role of resonators in the sound of mallet percussion instruments was the experimental work of Bork [8]. Here, Bork reports that the presence of tuned resonator tubes breaks the acoustic "short-circuit" of the dipole and increases the sound radiation of the bars at the fundamental frequency. However, the increased sound radiation is most often

* Corresponding author.
E-mail addresses: filipe.soares@ctn.tecnico.ulisboa.pt (F. Soares), jantunes@ctn.tecnico.ulisboa.pt (J. Antunes), vincentdebut@ipcb.pt (V. Debut).

https://doi.org/10.1016/j.apacoust.2022.109049
0003-682X/

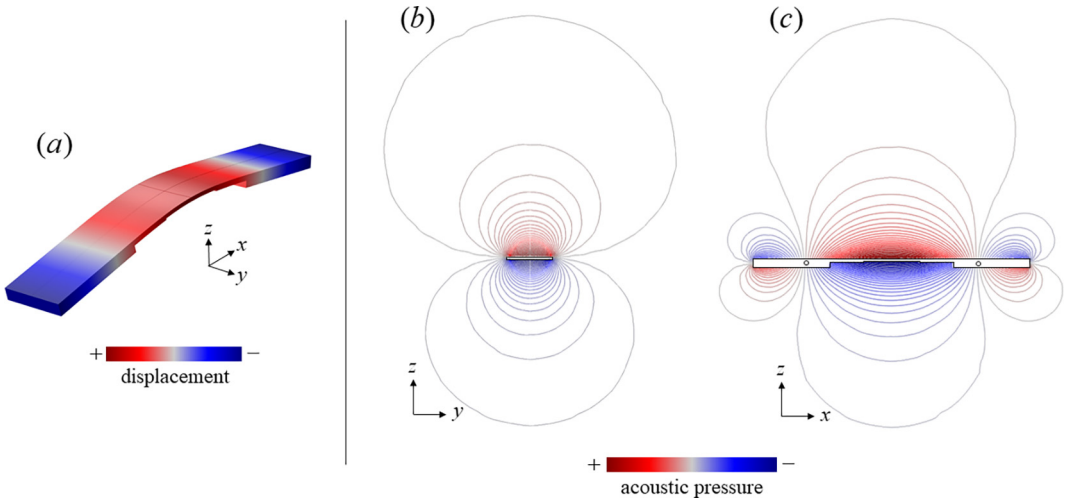

Fig. 1. (a) Mode shape of the first vertical bending mode of a typical bar with a (1:4:10) tuning ratio and the associated cross-sectional views of the acoustic radiation patterns in the (b) central $y-z$ plane and the (c) central $x-z$ plane.

accompanied by a significant decrease of the bar's decay time. This suggests that the role of resonators is to catalyze the conversion of vibrational energy of the bar into radiated acoustic energy.

Despite the knowledge gained from experimental reports [8,11], the development of models describing the acoustic-structure coupling between the bar and resonator are relatively rare in literature [12,13]. Here we underline the work of Chaigne and Doutant, that have numerically simulated 1-D bar vibrations through finite differences [14], and later extended the model to include sound radiation in the presence of a resonator [15]. Their modelling work deals with important aspects of the bar-resonator interaction. However, they considered coupling to occur only in one direction. That is, their model assumes that the back-coupling effect of the resonator on the bar vibration is negligible. This is in contradiction with experimental observations, which report significant changes to bar decay time when a tuned resonator is present [8,13].

To the authors knowledge, the only modelling work dealing with the two-way coupling dynamics between bars and resonators is the one recently published by Rucz et al. [13]. Here, the authors have used three-dimensional finite element models to describe the vibro-acoustic interaction as well as the sound pressure radiated into the free-field. The 3-D structural (bar) and acoustical elements (resonator and free field) are decomposed into a modal basis, which is then used in temporal integrations for a reduced computational cost. In general, their numerical results are in qualitative and quantitative agreement with experiments.

In this work, we present a simple and exploitable model describing the bar-resonator coupling dynamics. The bar is modelled as a disk-shaped oscillator, representing the vibrations of the first bending mode. The resonator is taken as a 1-D cylindrical acoustic waveguide, which is described in terms of its acoustic modes. The interaction between the disk and the resonator is calculated numerically via 2-D axisymmetric finite element (FE) models, whose results are then fitted to semi-empirical analytic formulas. This allows for the construction of a minimal lumped-parameter model, which is able to encapsulate the central aspects of the bar-resonator coupling dynamics.

In Section 2, we describe the dynamics of the two uncoupled mechanical and acoustical elements. In Section 3, the finite element model and ensuing numerical results are presented. Sections 4 and 5 describe the simplified coupled model and present numerical validation against results from a vibro-acoustic 2-D axisymmetric FE model. Sections 6 and 7 present an energy balance formulation and numerical results from the simplified model.

2. Model description

In traditional instruments, the most important coupling effects in bar-resonator interaction involve only the first bar mode. Therefore, we reduce the bar motion to a single mode. Moreover, since this mode radiates approximately as a dipole (Fig. 1), an attractive idea in the context of simplified approaches, is to describe the bar mode as a disk-shaped oscillator. A circular disk oscillating in free-space also radiates as a dipole (provided that the acoustic wavelength is much larger than the disk radius a). The disk is located at a distance d from the termination of an unbaffled cylindrical pipe of length L, of the same radius a, as illustrated in Fig. 2. The pipe is assumed closed at $x=0$ and open at $x=L$, with an associated acoustic radiation impedance Z_R.

2.1. Acoustics of the uncoupled resonator

In a one-dimensional domain, the small oscillations of a fluid about a state of rest can be described by the linearized Euler equations [16]. From these, we can derive the acoustic wave equation

$$\frac{1}{c^2}\frac{\partial^2 p(x,t)}{\partial t^2} - \frac{\partial^2 p(x,t)}{\partial x^2} = 0 \tag{1}$$

where $p(x,t)$ is the acoustic pressure and c is the speed of sound. At the closed end of the pipe ($x=0$), the particle velocity $u(0,t)$ is null and the boundary condition, in terms of acoustic pressure, becomes

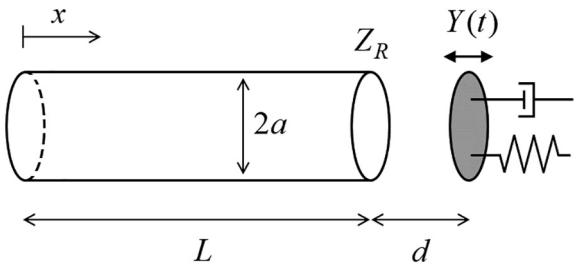

Fig. 2. Diagram of proposed 1-D model.

$$\left.\frac{\partial p(x,t)}{\partial x}\right|_{x=0} = 0 \tag{2}$$

At the open (unbaffled) end of the pipe ($x = L$) we impose the acoustic radiation impedance such that

$$Z_r = \frac{p\,(L,t)}{u\,(L,t)} \tag{3}$$

where we assume the impedance to be complex, containing both reactive and resistive terms. In the Laplace domain it can be represented, in general, by

$$Z_r = \rho c\left(s^2 R_r + sX_r\right) \tag{4}$$

where s is the complex Laplace variable, R_r and X_r are associated to the acoustic resistance and reactance, respectively. The boundary condition at $x = L$ becomes, in the Laplace domain,

$$p(L,s) + c(sR_r + X_r)\left.\frac{\partial p(x,s)}{\partial x}\right|_{x=L} = 0 \tag{5}$$

Using the method of separation of variables, we search for a general solution of the form $p(x,t) = \tilde{\phi}(x)g(t)$. Moreover, since there is a local dissipative condition at $x = L$ we search for the general solution in the complex space $\mathbb{C}$. Hence, we assume temporal solutions of in form $g(t) = e^{st}$, where $s \in \mathbb{C}$. After some algebraic manipulation, we arrive at the characteristic equation

$$\cosh\left(\frac{sL}{c}\right) + \left(s^2 R_r + sX_r\right)\sinh\left(\frac{sL}{c}\right) = 0 \tag{6}$$

whose solutions s_n are the complex eigenvalues of the uncoupled resonator. While difficult to solve analytically for a generic case, the solutions can be found numerically to obtain the real and imaginary parts of the eigenvalues $s_n = \alpha_n + j\omega_n$. Their physical interpretation is given by the following relations, in terms of the typical modal parameters

$$s_n = \bar{\omega}_n\zeta_n + j\bar{\omega}_n\sqrt{1-\zeta_n^2} \tag{7}$$

where the undamped natural frequencies $\bar{\omega}_n$ and damping ratio ζ_n are given by

$$\bar{\omega}_n = \sqrt{\alpha_n^2 + \omega_n^2} \qquad ; \qquad \zeta_n = \frac{\alpha_n}{\sqrt{\alpha_n^2 + \omega_n^2}} \tag{8}$$

Additionally, the complex mode shapes $\tilde{\phi}_n(x)$ are given as

$$\tilde{\phi}_n(x) = \cosh\left(\frac{s_n x}{c}\right) \tag{9}$$

2.1.1. Modal expansion of a conservative resonator

If we neglect the dissipative term in the radiation impedance $R_r = 0$, the characteristic equation is purely real (conservative system) and reduces to

$$\cot\left(\frac{\omega L}{c}\right) - \omega X_r = 0 \tag{10}$$

Moreover, since in realistic scenarios $\omega X_r \ll 1$, expression (10) is approximately equivalent to

$$\cot\left(\frac{\omega L}{c}\right) - \tan\left(\omega X_r\right) = 0 \tag{11}$$

whose solutions yield the classical "length correction" approximation of the eigenfrequencies $\bar{f}_n$ of the conservative pipe, given simply by

$$\bar{f}_n = \frac{\bar{\omega}_n}{2\pi} \approx \frac{c(2n-1)}{4(L+\Delta L)} \tag{12}$$

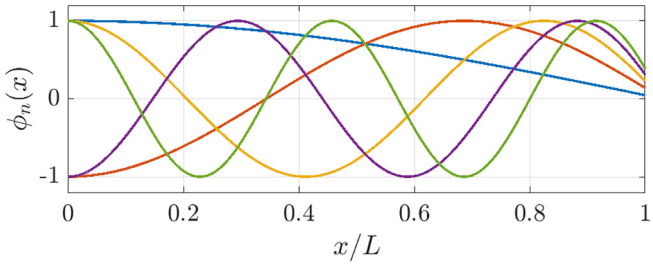

Fig. 3. Acoustic pressure mode shapes of a conservative resonator-pipe with closed-open (unbaffled) boundary conditions.

where the term $\Delta L = X_r c$ corresponds to the "length correction" term (for an unbaffled open end, $\Delta L = 0.6133a$ is a commonly used low frequency approximation). In this case, replacing $s_n = j\omega_n$ in (9), the modes shapes are purely real (Fig. 3) and given by

$$\phi_n(x) = \cos\left(\frac{\bar{\omega}_n x}{c}\right) \approx \cos\left(\frac{(2n-1)\pi}{2(L+\Delta L)}x\right) \tag{13}$$

Notice, in Fig. 3, that the mode shapes resemble that of an ideal closed-open pipe. However, in this case, there are no pressure nodes at $x = L$. At this point we can proceed with the modal decomposition of the problem. Developing the pressure field in terms of N mode shapes

$$p(x,t) = \sum_{n=1}^{N}\phi_n(x)q_n(t) \qquad \text{for} \quad n = 1,\ 2\ \ldots N \tag{14}$$

and substituting into the wave equation (1) leads to

$$\frac{1}{c^2}\sum_{n=1}^{N}\phi_n(x)\ddot{q}_n(t) - \sum_{n=1}^{N}\phi_n''(x)q_n(t) = 0 \quad \text{for} \quad n = 1,\ 2\ \ldots N \tag{15}$$

where the upper dash and dot denote differentiation with respect to space and time, respectively. Now, spatial integration in $0 \leqslant x \leqslant L$ and multiplication by $\phi_m(x)$, yields

$$\frac{1}{c^2}\sum_{n=1}^{N}\ddot{q}_n(t)\int_0^L \phi_n(x)\phi_m(x)dx - \sum_{n=1}^{N}q_n(t) \times \int_0^L \phi_n''(x)\phi_m(x)dx = 0 \quad \text{for} \quad \begin{cases} n = 1,\ 2\ \ldots N \\ m = 1,\ 2\ \ldots N \end{cases} \tag{16}$$

The second order spatial derivatives of the mode shapes $\phi_m''(x)$ are related to the actual mode shapes by

$$\phi_n''(x) = -\left(\frac{\bar{\omega}_n}{c}\right)^2\phi_n(x) \tag{17}$$

For non-ideal closed-open pipes, orthogonality does not strictly hold due to the effect of the length correction ΔL in the modes shapes (13). Assuming the typical length correction approximation $\Delta L = 0.6133a$, the terms stemming from the Galerkin projection, in dimensionless form (with $\bar{x} = x/L$), are given by

$$\int_0^1 \phi_n(\bar{x})\phi_m(\bar{x})d\bar{x} = \begin{cases} \dfrac{\sin(\alpha_n)}{2\alpha_n} + \dfrac{1}{2} & \text{for } m = n \\ \dfrac{\sin((\alpha_n-\alpha_m)/2)}{\alpha_n-\alpha_m} + \dfrac{\sin((\alpha_n+\alpha_m)/2)}{(\alpha_n+\alpha_m)} & \text{for } m \neq n \end{cases} \tag{18}$$

where the auxiliary parameter α_n (or equivalent for α_m) is given by

$$\alpha_n = \frac{\pi(2n-1)}{1 + 0.6133(a/L)} \tag{19}$$

However, for pipes that are not unreasonably wide ($a/L < 0.1$), the contributions of off-diagonal terms are small and the following (orthogonal) approximation is suitable

$$\int_0^L \phi_n(x)\phi_m(x)dx \approx \begin{cases} \frac{L+\Delta L}{2} & \text{for} \quad m=n \\ 0 & \text{for} \quad m\neq n \end{cases} \tag{20}$$

It is worth mentioning that in commercial instruments, resonator pipes with large aspect ratios $a/L > 0.1$ are rare, and occur only in highest register of some instruments (see [17] for example). Finally, after replacing (17) and (20) into (16), we can decouple the equations of motion into a set of N linearly independent modal equations

$$m_n\ddot{q}_n(t) + m_n\bar{\omega}_n^2 q_n(t) = 0 \quad \text{for} \quad n = 1,\ 2\ \ldots\ N \tag{21}$$

where the equivalent modal "inertial" coefficients are given by

$$m_n = \frac{L+\Delta L}{2c^2} \tag{22}$$

2.1.2. Modal expansion including radiation damping

When we account for the radiation damping, i.e. letting the radiation impedance have a positive real part R_r, the eigenfrequencies and modes shapes become complex, as stated above. Moreover, since the dissipative term is localized, this leads to a non-diagonal damping matrix $\boldsymbol{C}$, in the modal space. The presence of non-zero off-diagonal terms (inter-modal damping coefficients ζ_{mn}) formally prevents a decoupling of the equations of motion, as done above for the conservative case. Similar behavior can be found when modelling a string with a localized damper attached to one end (see for example [18]). However, if (1) modal damping is weak and (2) the eigenfrequencies are well separated, it can be demonstrated [18] that the inter-modal damping coefficients ζ_{mn} are negligible, and the damping matrix $\boldsymbol{C}$ is approximately diagonal. Moreover, the same conditions can be used to demonstrate that the first-order effect of inter-modal damping on the mode shapes is purely imaginary and of the same order of magnitude as the inter-modal damping coefficients. Therefore, the equations of motion for the dissipative system can be assumed decoupled while maintaining the real mode shapes of the equivalent conservative system, as demonstrated in detail in [18]. Under these simplifying, but reasonable, assumptions we get the modal equations

$$m_n\ddot{q}_n(t) + 2\zeta_n m_n\omega_n\dot{q}_n(t) + m_n\omega_n^2 q_n(t) = 0 \tag{23}$$

where the modal damping coefficients ζ_n (associated with radiation losses) are calculated through (8) after solving the characteristic equation. For simplicity, we will assume only the first bar mode radiates and only the first acoustic mode of the resonator is close enough in frequency for significant coupling effects to occur. The uncoupled resonator acoustics will thus be reduced to a single-degree-of-freedom system, i.e. $n = r = 1$.

2.2. Dynamics of the disk-oscillator

As mentioned previously, the bar will be modelled as a simple damped oscillator, describing the motion of the fundamental bar mode. Furthermore, we assume that the oscillator is shaped like a rigid circular disk. Its equation of motion is given by

$$m_s\ddot{Y}(t) + 2\zeta_s m_s\omega_s\dot{Y}(t) + m_s\omega_s^2 Y(t) = 0 \tag{24}$$

where m_s, ζ_s and ω_s are the modal mass, damping ratio and frequency of the first vertical-bending bar mode, respectively, and $Y(t)$ is the disk's vertical displacement.

It must be noted that fluid loading on the oscillator could easily be incorporated into the model by considering the radiation impedance of a freely suspended disk oscillating vertically in free-space, whose expressions can be found in classic acoustics textbooks like [19] or [20]. For example, in [21] we find the following low-frequency approximation (for $ka < 1$; where k is the wavenumber $k = \omega/c$), written in the frequency domain

$$Z_s(ka) = \frac{P_a(ka)}{\dot{Y}(ka)} = 2\rho c\left[j\left(\frac{4}{3\pi}\right)(ka) + \left(\frac{8}{27\pi^2}\right)(ka)^4\right] \tag{25}$$

where $P_a(t)$ is a pressure load acting on the disk by the surrounding fluid. Incorporation of this term, would lead to an added mass and damping terms to the disk's equation of motion

$$m_a = 2S\rho\left(\frac{4}{3\pi}\right)a \quad ; \quad \zeta_a = 2S\rho c\left(\frac{8}{27\pi^2}\right)\left(\frac{\omega_s a}{c}\right)^4 \tag{26}$$

where $S = \pi a^2$. The added mass term m_a would lower the natural frequency of the oscillator but, in light fluids, it is generally negligible compared to the mass of the structure. On the other hand, the added damping term ζ_a, which is associated with the energy dissipated through acoustic radiation, could eventually be useful in considerations regarding the radiated sound. However, for simplicity, in this work we will proceed without considering the fluid loading on the oscillator.

3. Finite element model & approximate formulae

The major difficulty in modelling the interaction between a vibrating beam and an acoustic resonator is associated with the three-dimensional effects of the acoustic radiation that couple the two mechanical-acoustical elements. Here, we search for analytical (semi-empirical) approximations that can, in a simplified manner, describe these effects. To this end, we make use of 2-D axisymmetric finite element (FE) models, whose results are then numerically fitted to simple analytical formulae that can be used in modelling framework described in the previous sections. In this section, FE models are used to (1) characterize the vibro-acoustic coupling between an oscillating disk and a cylindrical acoustic waveguide and (2) investigate the effect of a partial circular obstruction on the radiation impedance of a unflagged open pipe. The latter is motivated by the well-known phenomena that the presence of the bar above the resonator lowers its natural frequencies [8,13].

3.1. Acoustic radiation impedance of an unbaffled pipe with a partial circular obstruction

The mathematical modeling of the acoustic radiation from an unbaffled pipe is no trivial task. The first integral solution was famously derived by Levine and Schwinger in [22]. Since then, several (simpler) alternative formulations have been derived (e.g. [23]) which give reasonably accurate results in a wide frequency range ($ka < 3$). At this point is it worth noting that, in mallet percussion instruments, we typically find cylindrical resonators with radius 0.02 m $< a <$ 0.05 m, increasing in inverse proportion to pitch. Moreover, the highest fundamental frequency of a bar is typically around 2 kHz (musical note C7). Therefore, our range of interest will be for relatively low frequencies $ka < 1$ (worst case scenario). For most of the low and medium registers (up to 1 kHz), we will typically have $ka < 0.5$.

Perhaps the simplest and most commonly used form of the acoustic radiation impedance of an unbaffled cylindrical pipe, reasonable in the low frequency range ($ka < 1$), is given by

$$Z_R(\omega) = \frac{1}{4}(ka)^2 + j0.6133(ka) \quad , \quad for \quad ka < 1 \tag{27}$$

where $Z_R(\omega)$ is normalized by ρc. Fig. 4 shows the real and imaginary parts of $Z_R(\omega)$ given by a more precise model presented in [23] and the low-frequency approximation described above (27).

The formula presented above (27) may be a reasonable first approximation to what occurs in the resonators of mallet percus-

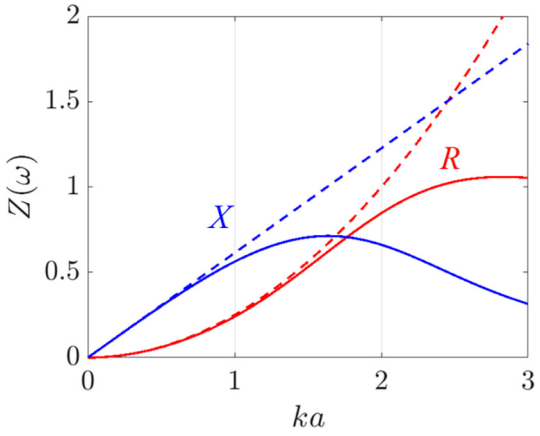

Fig. 4. Real and imaginary parts of the normalized acoustic radiation impedance from an unbaffled cylindrical pipe. The dashed lines show the low-frequency approximation given in (27) while solid lines show results from a more accurate model described in [23].

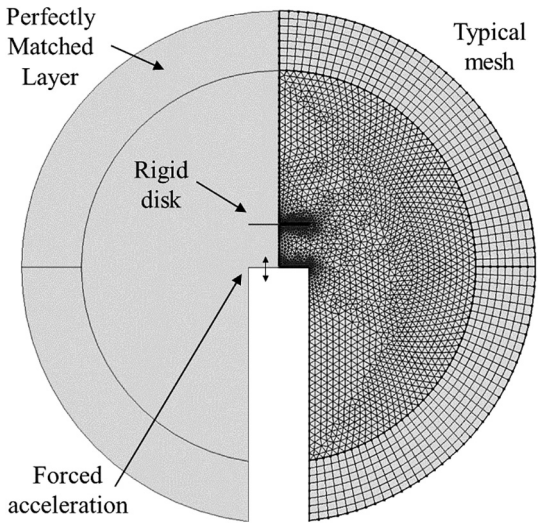

Fig. 5. Illustration of the 2-D axisymmetric finite element model and a typical mesh.

sion instruments. However, the presence of the bar above the termination of the resonator will affect its radiation impedance. This phenomenon is well-known to builders and typically leads to a noticeable decrease in the natural frequencies of the resonator [8]. In [24], Rucz et al. present a study where the radiation impedance of a closed-open (baffled) cylindrical resonator obstructed by a bar was calculated numerically via 3D finite element models. They present illustrative results underlining variations of relevant dimensionless quantities: the bar-resonator distance d/a, the ratio of bar width to resonator radius w/a, as well as the inclusion of adjacent bars. However, analytical expressions for the radiation impedance in terms of these parameters are not presented. Here, we simplify the geometry of the problem further by assuming the bar presence can be approximately described by a rigid circular disk of the same radius a, with the aim of providing a simplified expression for the radiation impedance in terms of the sole two dimensionless parameters: the frequency ka and the disk-resonator distance d/a. This geometric simplification is justified by: (1) the thickness of bar has negligible effect [24]; (2) in realistic scenarios the bar width is equal to (or very near) the resonator diameter; and (3) the bar length is likely to have a minor effect as the smallest dimension of the obstruction (in this case the bar width) will typically have a dominant role.

The 3D finite-element model, illustrated in Fig. 5, consisted of a 2-D axisymmetric domain surrounded by Perfectly Matched Layers (PML) to simulate anechoic conditions. A cylindrical pipe is terminated by an unbaffled open-end and a rigid circular disk (infinitely thin) is located at a distance d above the pipe termination. Acoustic plane waves are forced at the termination of the pipe by a unitary prescribed acceleration.

The meshing of the central domain consisted of unstructured second-order triangular elements, while the PMLs are meshed in a structured manner using second-order quadrilateral elements. The maximum element size was set to a tenth of the smallest wavelength considered $h_{\max} = \lambda_{\min}/10$, and the region near the pipe termination was refined for increased accuracy at this crucial location. The model is solved in the frequency domain (Helmholtz equation) and the radiation impedance is calculated by the ratio of the spatial integrals of the normal particle velocity and pressures fields at the pipe termination surface. The estimation of the radiation impedance of resonators from FE numerical results can be calculated more precisely with other methods [25]. However, the present approach is deemed adequate in the (low-frequency) context of this work.

Fig. 6 below shows the numerical results for the real and imaginary parts of the calculated radiation impedance for various values of the dimensionless disk distance d/a, in the frequency range $ka < 3$.

The peaks seen at the high-frequency range are associated with radial resonances appearing when the distance d is comparable with the wavelength $\lambda = c/\omega$. In any case, we are not interested in this high-frequency behavior as mentioned above. In the lower frequency range ($ka < 1$), numerical results suggest that:

1. The acoustic resistance $R_R = Re(Z_R)$ is virtually unchanged by the presence of the disk.
2. The acoustic reactance $X_R = Im(Z_R)$ remains approximately linearly dependent on ka, and its slope increases with decreasing d/a.

Similar conclusions can be found in the results presented in [24]. To formulate a low frequency approximation, we first assume that the acoustic resistance remains unchanged. This is equivalent to say that, in the low frequency range, the amount of radiated acoustic energy is independent of the obstruction distance d. Secondly, the slopes of the imaginary part of the acoustic reactance $\partial Im(Z)/\partial(ka)$ can be approximated by a simple linear regression. Taking as a starting point, the radiation impedance of an unobstructed pipe (27), the resulting slopes fitted to the FE results suggest that the acoustic reactance can be approximated by the following expression in terms of the dimensionless disk distance d/a

$$Im\,(Z_R) = \left(\beta\frac{a}{d}+1\right)0.6133(ka) \tag{28}$$

where the parameter β was fitted numerically to give $\beta \approx 0.32$, as illustrated in Fig. 7. Therefore, a low frequency approximation of the acoustic radiation impedance of a unbaffled cylindrical pipe with a rigid circular obstruction is given by

$$Z_R(\omega, d) = \frac{1}{4}(ka)^2 + j\left(\beta\frac{a}{d}+1\right)0.6133(ka) \tag{29}$$

Notice that when $d \to \infty$ the radiation impedance converges to that of an open unbaffled pipe (27). When $d \to 0$, the imaginary part goes to infinity, as that of a closed pipe. Here, the value of β is based on the assumption that the presence of the bar can be roughly described by a rigid circular disk whose diameter is equal to the

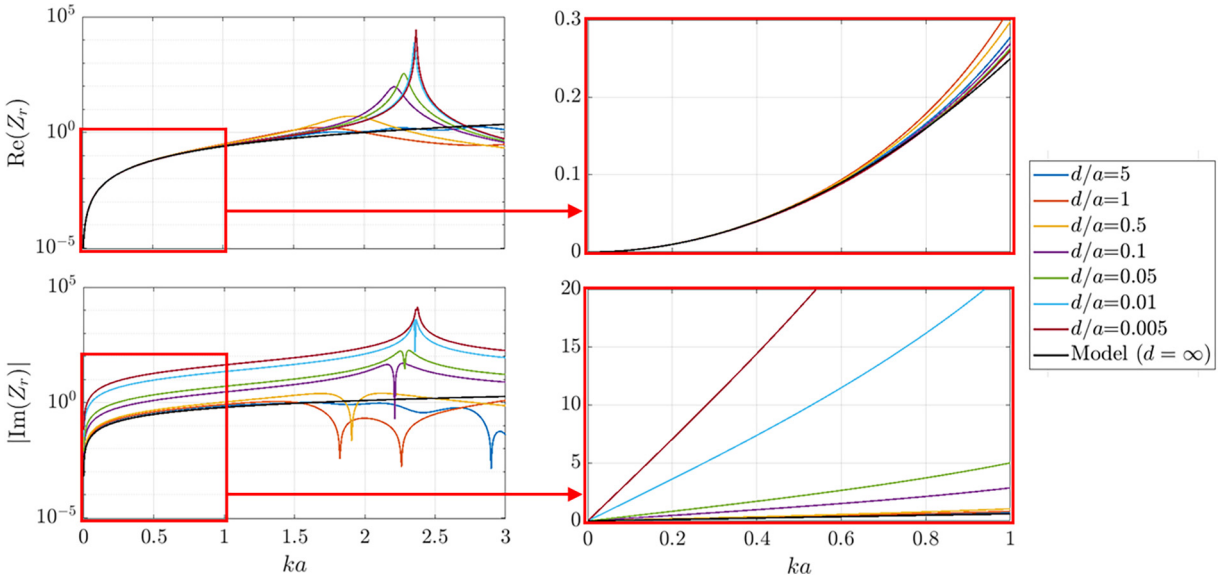

Fig. 6. Real and imaginary (absolute) parts of the normalized radiation impedance of a unbaffled pipe with circular rigid obstruction, calculated with the FE model for various values of (normalized) disk distance d/a. The left plots show the impedance in the frequency range $ka < 3$, in a logarithmic scale, while the plots on the right show results in the range $ka < 1$, in a linear scale.

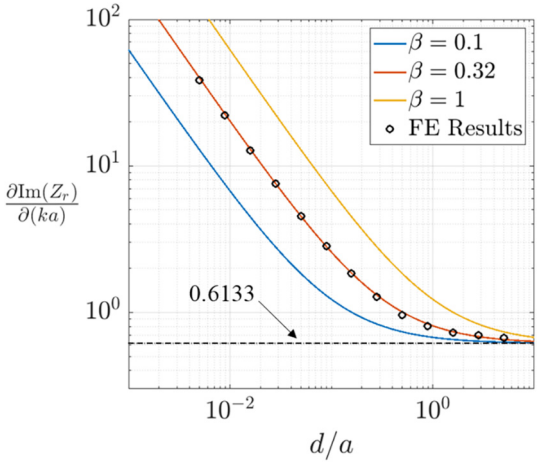

Fig. 7. Analytical low frequency approximation of the slopes of the numerically calculated acoustic reactance $X_R(ka)$.

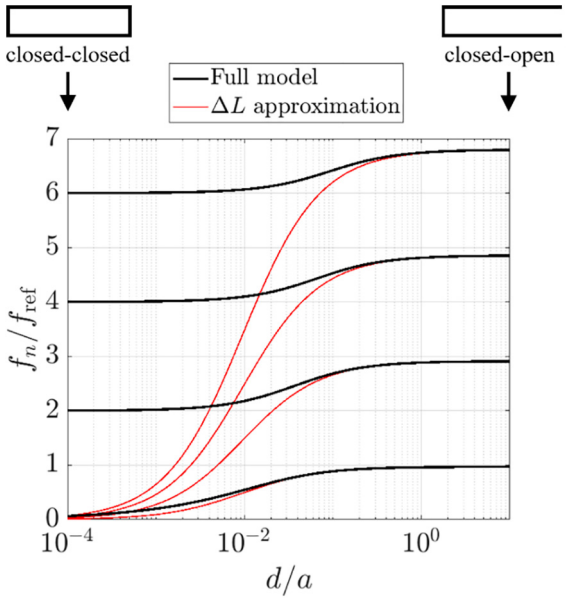

Fig. 8. Evolution of (normalized) resonant frequencies as a function of disk distance d for a tube with length/radius ratio $a/L = 0.05$. Here, $f_{ref} = c/4L$.

bar's width. However, better approximations for this value can probably be achieved by fitting β to experimental results using real bars. Since real bars occupy larger areas above the pipe, it is likely that $\beta < 0.32$ in realistic scenarios.

Then, replacing the radiation impedance expression (29) in the characteristic equation derived earlier (6) will yield the modified modal frequencies and damping ratios. Moreover, provided that d is not unreasonably small ($d/a > 0.1$), we can follow the simplification procedure used earlier, and derive a "length correction" approximation of the modal frequencies of the acoustic resonator

$$f_n = \frac{c(2n-1)}{4\left[L + \left(\beta\frac{a}{d} + 1\right)0.6133a\right]} \tag{30}$$

For illustration, Fig. 8 shows the evolution of the modal frequencies f_n of a pipe with $a/L = 0.05$, as a function of the nondimensional disk distance d/a. The black lines describe the resonant frequencies calculated with the characteristic equation while the red lines show the "length correction" approximation given by (30). Notice how, when d/a is large, the frequencies tend to those of a closed-open (unbaffled) pipe, while when $d \to 0$ the frequencies converge to those of an ideal closed-closed pipe.

3.2. Vibro-acoustic coupling

In the context of mallet percussion instruments, the structural and acoustic elements are not directly linked, since the termination of the resonator is at $x = L$ and the disk-oscillator (beam) is located at $x = L + d$. Therefore, we will model their interaction in terms of mutual excitations. That is, from one hand, the acoustic energy radiating from the pipe termination ($x = L$) will induce a pressure load on the disk and, on the other hand, the motion of the disk will radiate acoustic energy which will excite the resonator. Therefore, we aim to find transfer functions that relate: (1) the pressure at the

pipe termination to the induced pressure on the disk, and (2) the motion of the disk to the equivalent acoustic excitation at the pipe termination.

On this point, we remind the reader of the principle of vibro-acoustical reciprocity. Nowadays, this is a well-established concept, formally demonstrated by Lyamshev in 1959 [26] and developed further in the works of Wolde et al. [27,28], Fahy [29,30], amongst others. In its simplest form, the vibro-acoustical reciprocity is expressed as

$$\frac{p_i}{\ddot{Y}_j} = \frac{f_j}{\dot{q}_i} \tag{31}$$

where p_i is a response pressure within the acoustic domain, f_j is a force load excitation on the structure, Y_j is a displacement on the structure and q_i is an acoustic excitation (in terms of volume velocity). In words, relation (31) states that the transfer function between the motion of a structure $\ddot{Y}_j$ at point j and a response pressure p_i in the acoustic domain at point i, is equivalent to the transfer function between an acoustic source $\dot{q}_i$ at point i and the force load on the structure at point j, as illustrated in Fig. 9.

The principle of vibro-acoustic reciprocity can be rearranged as a dimensionless transfer function. In the context of our system, this can be written in the frequency domain as

$$H(\omega) = \frac{F_{rs}(\omega)}{p(L,\omega)S} = \frac{\dot{Q}_{sr}(L,\omega)}{\ddot{Y}(\omega)} \tag{32}$$

where $F_{rs}(t)$ is a (spatially averaged) force induced on the disk by the acoustic waves leaving the resonator and $\dot{Q}_{sr}(t)$ is an acoustic excitation (in terms of volume acceleration) induced on the resonator by the disk motion. Then, with the knowledge of $H(\omega)$, the terms $F_{rs}(\omega)$ and $\dot{Q}_{sr}(\omega)$ can be calculated and used as forcing terms in the equations of the disk (24) and of the resonator (23), respectively.

Using an FE model similar to the one described earlier, the transfer function $H(\omega)$ can easily be estimated. For simplicity, we have considered two parallel circular surfaces (of the same radius a) separated by a distance d/a, as illustrated in Fig. 10.

The transfer function $H(\omega)$ was calculated numerically by relating the forced acceleration at the top surface ($\ddot{Y}(\omega)$) to the spatial integral of the acoustic volume acceleration felt at the bottom surface $\dot{Q}_{sr}(\omega)$. The FE numerical results for the transfer function $H(\omega)$ at various distances d/a are shown in Fig. 11, in term of its modulus $|H(\omega)|$ and phase $\angle H(\omega)$.

At relatively low frequencies ($ka < 1$), the modulus $|H(\omega)|$ remains approximately constant with respect to nondimensional frequency ka. Furthermore, when $d/a \to 0$, $|H(\omega)| \to 1$; and when $d/a \to \infty$, $|H(\omega)| \to 0$, as one would expect. The phase $\angle H(\omega)$ is nearly linear, with slope $\partial\angle H(\omega)/\partial ka$ decreasing as d/a increases. Effectively, this nearly linear phase-shift can be regarded as a time delay in the response associated with the travelling acoustic waves. Therefore, at relatively low frequencies ($ka < 1$), the transfer function $H(\omega)$ could be approximated as simple constant gain filter with a time delay τ. Then, the mutual excitations can be calculated in the time domain by

$$\dot{Q}_{sr}(L, t+\tau) = |H(\omega)|\ddot{Y}(t) \tag{33}$$

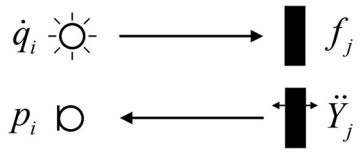

Fig. 9. Illustrative diagram of the principle of vibro-acoustic reciprocity.

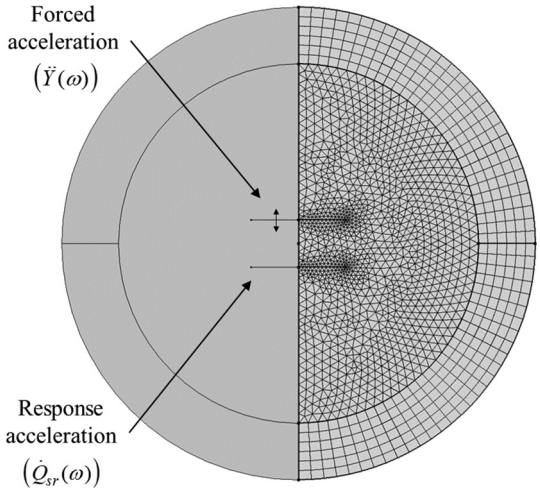

Fig. 10. Illustration of the FE model used to estimate the vibro-acoustic transfer function $H(\omega)$.

$$F_{rs}(t+\tau) = |H(\omega)|p(L,t)S \tag{34}$$

where the time delay τ could be roughly approximated by $\tau = d/c$. However, since the distance d will generally be much smaller than the considered wavelengths, $d \ll c/\omega$, we can neglect this time delay in a first approximation. This simplification assumes that the dynamics at one surface will be felt instantaneously at the other surface. Then, neglecting the phase-shift and assuming a modulus which is constant in frequency, we can search for an analytical approximation which depends only on the dimensionless distance d/a. Here, we search for an approximate function in the following polynomial form

$$H(d/a) = \frac{1}{1 + \alpha_1(d/a) + \alpha_2(d/a)^2 + \ \ldots\ + \alpha_p(d/a)^p} \tag{35}$$

Note that the above expression is coherent with the expected limiting values mentioned above: (1) if $d/a \to 0$, $H \to 1$; and (2) if $d/a \to \infty$, $H \to 0$. The values of $|H(\omega \to 0)|$ obtained with the FE model were taken as the target values and the polynomial function (35) was numerically fitted (least-squares), to obtain the coefficients α_p which better approximate the FE data. Results for the numerical fitting are shown in Fig. 12, assuming polynomials of various orders p. The resulting values of the polynomial coefficients α_p, are shown in Table 1. In the following sections, we will use the 5th order approximation of $H(\omega)$ throughout. As a note, subsequent to the conclusion of this work, an analytical formulation for calculation of the self and mutual radiation impedances of spheroids has been published [31]. This method can potentially be used to provide additional accuracy to the model, particularly at higher frequencies.

4. Formulation of the coupled system

Following the above estimated transfer function (35), the force load on the disk, induced by the resonator is then given by

$$F_{rs}(t) = Hp(L,t)S = H\phi(L)q(t)S \tag{36}$$

The equation of motion of the disk-oscillator then becomes

$$m_s\ddot{Y}(t) + 2\zeta_s m_s\omega_s\dot{Y}(t) + m_s\omega_s^2 Y(t) = H\phi(L)q(t)S \tag{37}$$

The inhomogeneous acoustic wave equation can be formulated by adding a sound source term, in terms of a pressure gradient or volume acceleration $\dot{Q}_{sr}(t)$ [32]. After projection unto the acoustic modes, the resonator equation becomes

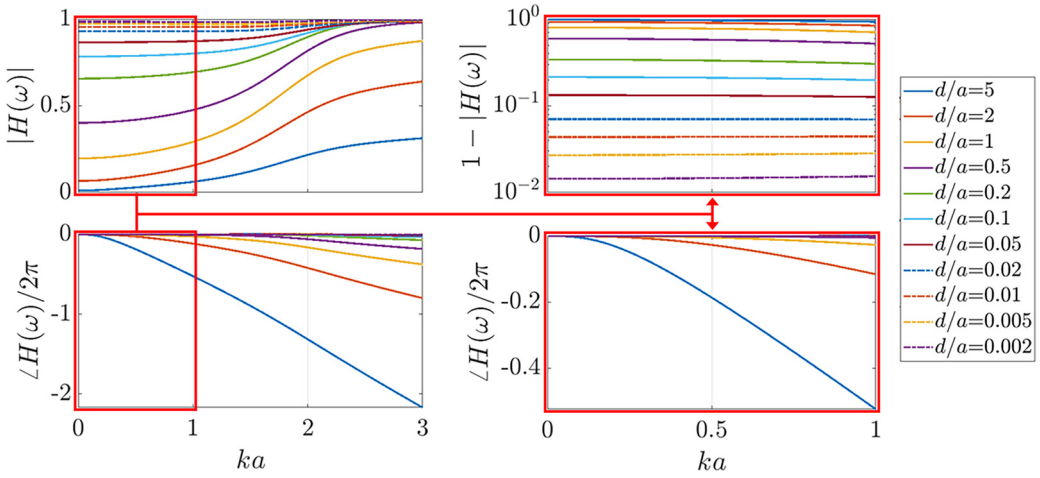

Fig. 11. Finite element computation of the magnitude and phase of the transfer function $H(\omega)$ as a function of ka, for various values of the nondimensional distance parameter d/a. The in the top-right plot, the magnitude is represented by the function $1-|H(\omega)|$ in a logarithmic scale, for clarity.

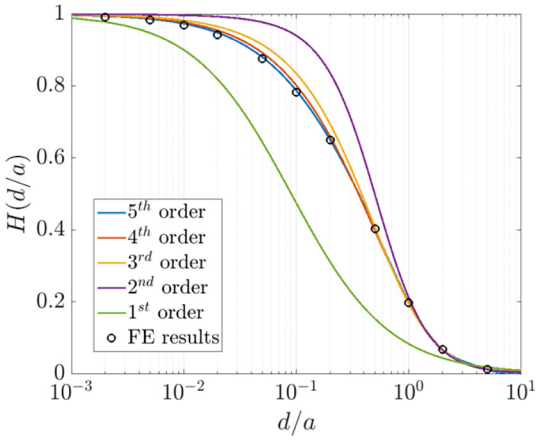

Fig. 12. Comparison between the low frequency approximation of the function $H(\omega)$ calculated by the FE model and polynomial approximations of various orders.

Table 1
Values of the best fitted polynomial coefficients α_p, for various polynomial orders.

Model order	α_1	α_2	α_3	α_4	α_5
5th order	2.778	−1.033	3.345	−1.151	0.128
4th order	2.373	0.906	0.864	−0.088	
3rd order	1.762	2.203	0.189		
2nd order	0.296	3.439			
1st order	11.156				

$$m_1\ddot{q}(t)+2\zeta_1 m_{11}\dot{q}(t)+m_1\bar{\omega}_1^2 q(t) = \rho\dot{Q}_{sr}(t)\int_0^L \delta(x-L)\phi(x)dx \tag{38}$$

and simplifying the spatial integral and using relation (33), the equation reduces to

$$m_1\ddot{q}(t)+2\zeta_1 m_1\bar{\omega}_1\dot{q}(t)+m_1\bar{\omega}_1^2 q(t)=\rho H\phi(L)\ddot{Y}(t) \tag{39}$$

Finally, the coupled system can be written in matrix form as

$$\begin{bmatrix} m_s & 0 \\ \Pi_1 & m_r \end{bmatrix}\begin{Bmatrix}\ddot{Y}(t)\\ \ddot{q}(t)\end{Bmatrix}+\begin{bmatrix} c_s & 0 \\ 0 & c_r \end{bmatrix}\begin{Bmatrix}\dot{Y}(t)\\ \dot{q}(t)\end{Bmatrix}+\begin{bmatrix} k_s & \Pi_2 \\ 0 & k_r \end{bmatrix}\begin{Bmatrix}Y(t)\\ q(t)\end{Bmatrix}=\begin{Bmatrix}0\\0\end{Bmatrix} \tag{40}$$

where

$$\begin{aligned} k_s &= m_s\omega_s^2 \quad ; \quad k_r = m_1\bar{\omega}_1^2 \\ c_s &= 2\zeta_s m_s\omega_s \quad ; \quad c_r = 2\zeta_1 m_1\bar{\omega}_1 \\ \Pi_1 &= H\phi(L)\rho \quad ; \quad \Pi_2 = -H\phi(L)S \end{aligned} \tag{41}$$

Notice that both coupling terms depend on $H(d)$, and since $d\to\infty$ means $H\to 0$, the oscillators are effectively decoupled if the disk is sufficiently far away. Even though the coupling is reciprocal, the resulting coupled system (40) is not symmetric. In fact, this formulation is a typical result of vibro-acoustic coupling when acoustic pressure is used as the field variable [33–36]. Nevertheless, a different choice of acoustic variable can lead to symmetric formulations, which are often more practical in various applications. For example, if the acoustics are described in terms of particle displacement $w(x,t)$, the coupled system becomes symmetric and inertially coupled. That is, expanding the particle displacement field as

$$w(x,t)=\sum_{n=1}^{N}\psi_n(x)\xi_n(t) \quad \text{where} \quad \psi_n(x)=\sin\left(\frac{\bar{\omega}_n x}{c}\right) \tag{42}$$

the coupled system becomes

$$\begin{bmatrix} m_s & \Pi \\ \Pi & m_r \end{bmatrix}\begin{Bmatrix}\ddot{Y}(t)\\ \ddot{\xi}(t)\end{Bmatrix}+\begin{bmatrix} c_s & 0 \\ 0 & c_r \end{bmatrix}\begin{Bmatrix}\dot{Y}(t)\\ \dot{\xi}(t)\end{Bmatrix}+\begin{bmatrix} k_s & 0 \\ 0 & k_r \end{bmatrix}\begin{Bmatrix}Y(t)\\ \xi(t)\end{Bmatrix}=\begin{Bmatrix}0\\0\end{Bmatrix} \tag{43}$$

where, in this formulation, the symmetric coupling term Π and the "modal inertia" of the acoustic mode m_r are modified to

$$\Pi = H\left(\frac{c}{\bar{\omega}_r}\right)\phi(L)\rho S \quad ; \quad m_r=\frac{\rho S(L+\Delta L)}{2} \tag{44}$$

5. Numerical validation

Finally, we now want to numerically validate results of our simplified analytical model with the use of a more detailed 2-D axisymmetric model which includes the acoustic-structure interaction between the disk-oscillator and the resonator. To this end a new FE model was formulated, similar to those described above, where now we associate to the rigid circular disk a mass m_s, a stiffness k_s and a damping coefficient c_s, as illustrated in Fig. 13. The disk motion is restricted to one direction.

For comparison purposes, we now solve the FE model for the associated eigenvalue problem to assert the resulting coupled modes between the resonator (first acoustic mode) and the disk-

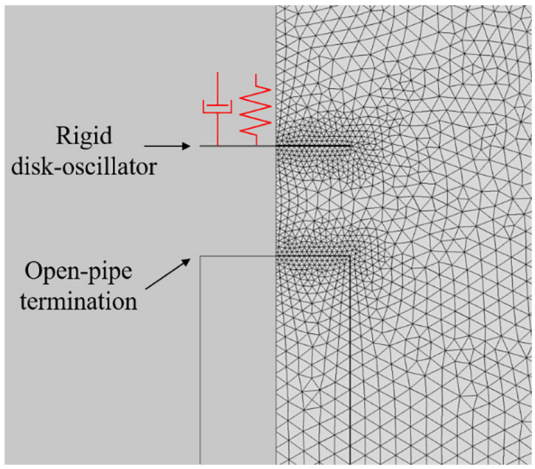

Fig. 13. Illustration of the FE model describing the acoustic-structure interaction, using a rigid disk with associated mass, stiffness and damping.

oscillator (first beam mode). These results can then be compared to the eigenvalues resulting from our simplified analytical model.

To maintain a consistent mesh, a parametric sweep was performed on the natural frequency of the disk-oscillator by modifying the associated stiffness k_s. The natural frequency of the disk was swept across the region near the frequency of the first acoustic mode of the resonator. The mass of the disk was maintained constant at $m_s = 0.2$ kg and the associated modal damping was set to $\zeta_s = 0.05\%$. These values are in the same order of magnitude of those found for the first bending mode of a vibraphone bar, made of aluminum. The length of the resonator was fixed at $L = 0.5$ m, and 3 different pipe radiuses were considered: (1) $a/L = 0.2$, (2) $a/L = 0.05$ and (3) $a/L = 0.02$. The resulting complex eigenvalues from the FE model and the analytical model are represented in Fig. 14, Fig. 15 and Fig. 16, for the wide, medium and narrow pipes, respectively, at different disk distances d/a. The imaginary part of the eigenvalues is represented by the damped natural frequencies f_n, while the real part as the damping ratios ζ_n.

The behavior of the coupled system is similar to other systems commonly found in musical acoustics. For example, the analysis in [37] can be very instructive, where a model of the coupling between a string and a soundboard (single-mode) yields results very similar to those above. We notice that the two eigenvalues cross when the frequency ratio (frequencies of the uncoupled oscillators f_s/f_r) equals to one, i.e. when the two oscillators are perfectly tuned. Depending on the "coupling strength"Π, the eigenvalues can cross in their real or imaginary part. When coupling is strong (low d/a), the eigenvalues cross in the real part and the two modes vibrate at different frequencies, but with the same damping ratio $\zeta_{1,2} \approx (\zeta_r + \zeta_s)/2$. When coupling is weak (large d/a), the eigenvalues cross in the imaginary part and the two modes vibrate at the same frequency, with distinct damping.

Aside from some minor quantitative differences, the analytical model is able to portrait the coupling dynamics of the two oscillators in a remarkably accurate manner.

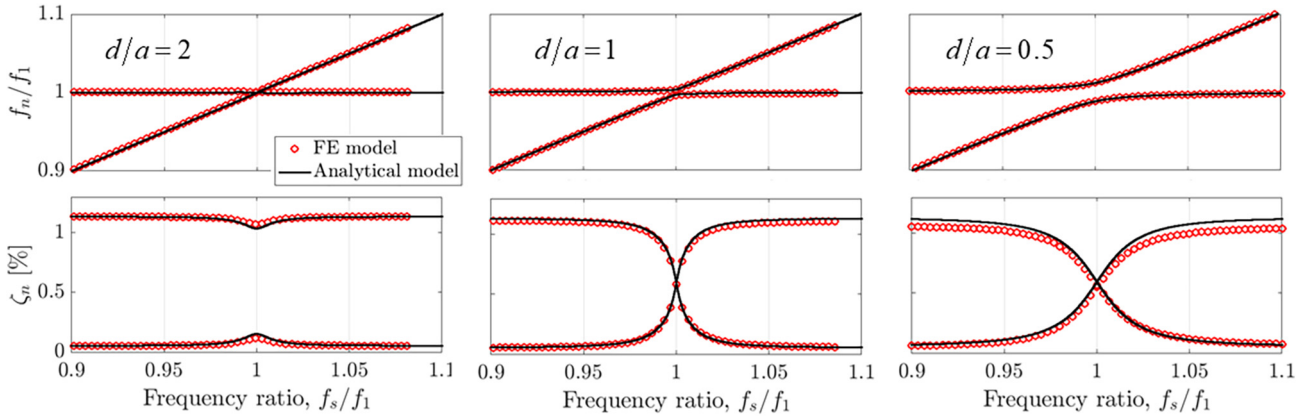

Fig. 14. Eigenvalue evolution as a function of the frequency ratio f_s/f_1, for the wide pipe with $a/L = 0.2$. Comparison between the results from the FE model and the analytical model.

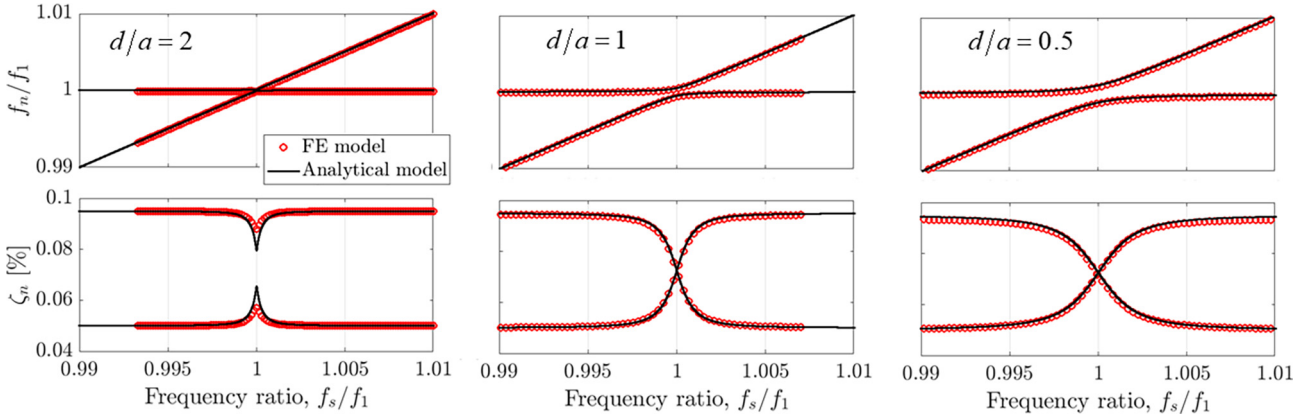

Fig. 15. Eigenvalue evolution as a function of the frequency ratio f_s/f_1, for the medium pipe with $a/L = 0.05$. Comparison between the results from the FE model and the analytical model.

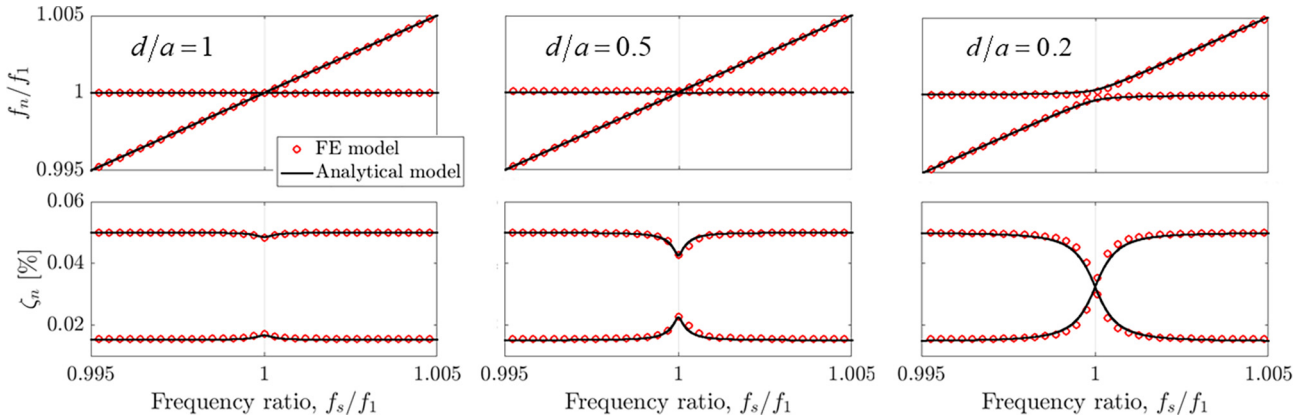

Fig. 16. Eigenvalue evolution as a function of the frequency ratio f_s/f_1, for the narrow pipe with $a/L = 0.02$. Comparison between the results from the FE model and the analytical model.

6. Energy balance

To analyze the behavior of the coupled system it is useful to have an energetic balance of the different subsystems as well as relevant parameters like radiation efficiency or decay time. Here, we make use of the formulation using particle displacement as the acoustic variable. The potential and kinetic energies, $U_s(t)$ and $T_s(t)$, in the disk-oscillator are given by

$$T_s(t) = \frac{m_s}{2}\dot{y}^2(t) \quad ; \quad U_s(t) = \frac{k_s}{2}y^2(t) \tag{45}$$

while the total amount of energy dissipated by the disk via internal losses $D_s(t)$ is given by

$$D_s(t) = c_s \int_0^t \dot{y}^2(t)\, dt \tag{46}$$

Similarly, the potential and kinetic energies of the resonator, $U_r(t)$ and $T_r(t)$, are calculated by

$$T_r(t) = \frac{m_r}{2}\dot{\xi}^2(t) \quad ; \quad U_r(t) = \frac{k_r}{2}\xi^2(t) \tag{47}$$

while the dissipated energy (acoustic radiation from the pipe's open end) is given by

$$D_r(t) = c_r \int_0^t \dot{\xi}^2(t)\, dt \tag{48}$$

Then, the energy stored in the coupled system is given by

$$E_C(t) = T_s(t) + U_s(t) + T_r(t) + U_r(t) \tag{49}$$

while the total dissipated energy is given by

$$D_C(t) = D_s(t) + D_r(t) \tag{50}$$

By energy conservation, and under free vibration conditions, the following relation expressing the total energy in the system holds

$$E_T = T_s(t) + U_s(t) + T_r(t) + U_r(t) + D_s(t) + D_r(t) = \text{constant} \tag{51}$$

In the context of free vibrations, a useful indicator of the impact of the resonator can be given by a "radiation efficiency" parameter κ, representing the percentage of energy in the system that is dissipated through the acoustic radiation by the resonator

$$\kappa = \frac{D_r(t=+\infty)}{E_T} \times 100 \quad [\%] \tag{52}$$

Similarly, we define the decay time of the coupled system, t_{60}, as the time it takes for its energy to decay by 60 dB (to 0.1 % of its the initial energy), that is

$$20\log_{10}\left(\frac{E_C(t_{60})}{E_C(0)}\right) = -60 \text{ dB} \iff \frac{E_C(t_{60})}{E_C(0)} = 0.001 \tag{53}$$

7. Illustrative numerical results

To illustrate how the system behaves in the time-domain, we show here temporal integrations of a system with the following parameters: $m_s = 0.2$ kg, $\zeta_s = 0.02\,\%$, $a = 0.03$ m, $L/a = 15$, $d/a = 0.5$, $\rho = 1.2$ kg $\cdot\, m^{-3}$ and $c = 340$ m $\cdot\, s^{-1}$. The coupling strength $H(d/a)$ is as defined in (35), using the 5th-order polynomial approximation. The resonator radiation impedance Z_R is as defined in (29) with $\beta = 0.32$, leading to: $f_r = 181.5$ Hz, $\zeta_r = 0.16\,\%$ and $m_r = 0.8 \times 10^{-3}$ kg (using the particle displacement formulation, Eq. (43)). This parameter configurations approximates what would be found in the lower register of a vibraphone.

The temporal integrations were performed using Matlab's Ordinary Differential Equation (ODE) solver, ode23t [38]. Initial conditions were set with the resonator at rest $\xi(0) = \dot{\xi}(0) = 0$, and the disk-oscillator was given an initial velocity, i.e. $y(0) = 0$ and $\dot{y}(0) = 1$ m $\cdot\, s^{-1}$. Fig. 17 shows the response of the resonator $\xi(t)$,

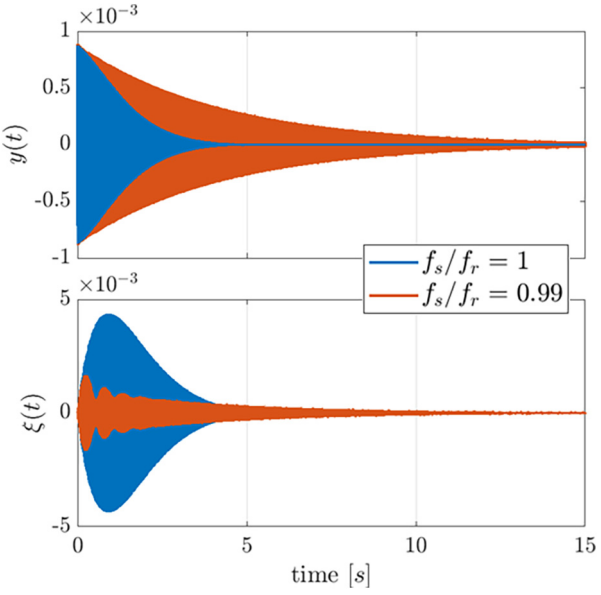

Fig. 17. Temporal evolution of the disk displacement $y(t)$ and resonator response $\xi(t)$, for different beam-resonator tuning ratios f_s/f_r.

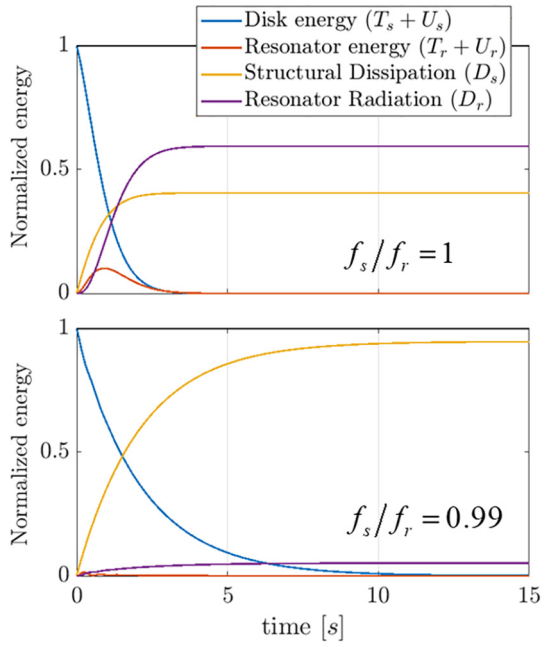

Fig. 18. Distribution of the energy in the coupled system for the three tuning cases. All values are normalized by the initial energy, i.e. $E_i(0) = T_s(0) = m_s/2$.

and the disk-oscillator displacement $y(t)$, for two different tuning ratios $f_s/f_r = [0.99,\ 1]$. Additionally, Fig. 18 shows the distribution of energy within the system as a function of time, for the tuned and untuned cases.

The results in Fig. 17 illustrate clearly that a perfectly tuned beam-resonator system leads to a stronger coupling between the two elements, and the resonator (initially at rest) is strongly excited, as expected. Consequently, we see a more rapid decrease of the disk vibration, a phenomenon commonly reported in experimental observations [8,13]. The same effect can be seen in the energy distributions shown in Fig. 18. For the tuned case ($f_s/f_r = 1$), the vibrational energy in the disk-oscillator is reduced to less than 1 % of its initial value in only 3 s, compared to about 10 s for the untuned case ($f_s/f_r = 0.99$). On the other hand, notice that in the tuned case, most of the energy is dissipated through the acoustic radiation of the resonator, while structural dissipation is dominant in the untuned case.

To examine in more detail the effect of tuning as well as the effect of the distance d on the coupling dynamics, multiple temporal simulations were conducted using various pairs of tuning ratio f_s/f_r and disk distance d, for the same system parameters as above. Fig. 19 shows the variation of radiation efficiency κ and the decay time t_{60}, as a function of the tuning ratio, for various values of the distance d.

The results shown in Fig. 19 demonstrates the typical compromise between acoustic radiation and decay time. Similar results can be seen in the experimental and theoretical works of Bork [8] and Rucz et al. [13]. Not surprisingly, we notice that decreasing the distance between disk and the resonator results in a stronger coupling, which further emphasizes this compromise. Here it must be noted that the above-mentioned behavior is associated with a particular bar-resonator configuration, namely, one in which the damping ratio of the structural element is smaller than the radiation damping of the resonator, i.e. $\zeta_s < \zeta_r$. Undoubtably, this is a scenario often encountered in metallic instruments. However, in some wooden instruments, it might be the case that structural damping of the bar mode is larger than the resonator damping, $\zeta_s > \zeta_r$. To illustrates the differences, we show in Fig. 20 the decay time and radiation efficiency for a similar set-up as above, except

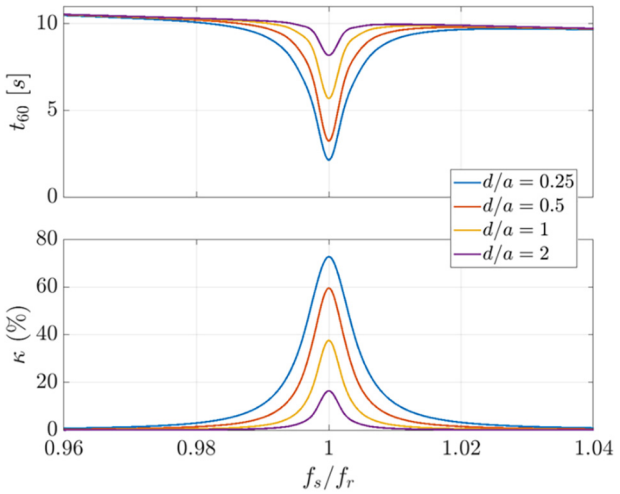

Fig. 19. Decay time t_{60}, and radiation efficiency κ, as a function of tuning ratio, for various values of nondimensional disk distance d/a, in a system where structural damping is lower than the resonator damping, $\zeta_s < \zeta_r$.

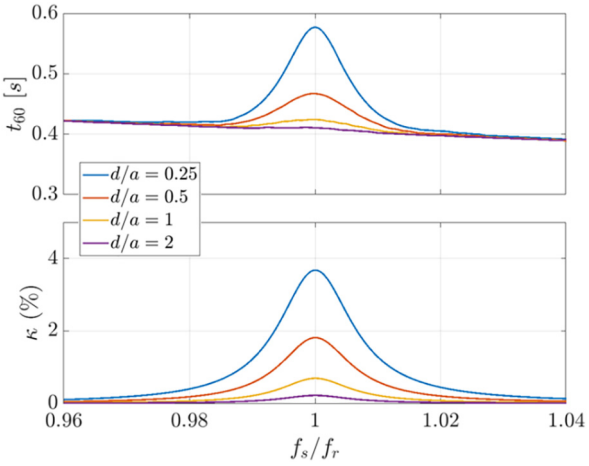

Fig. 20. Decay time t_{60}, and radiation efficiency κ, as a function of tuning ratio, for various values of nondimensional disk distance d/a, in a system where structural damping is larger than the resonator damping, $\zeta_s > \zeta_r$.

the structural damping is now set to $\zeta_s = 0.5\%$, as might be found in marimbas or xylophones [39,8].

In this case, we notice that coupling with the resonator results in both an increase of the radiation efficiency as well as in the decay time of the coupled system. Results suggest that, unlike in metallic instruments (where generally $\zeta_s < \zeta_r$), a compromise between decay time and radiation efficiency might not be necessary in some wooden instruments (where $\zeta_s > \zeta_r$) and the presence of the resonator could serve to increase both radiation efficiency and decay time. To the authors knowledge, this behavior has not been validated experimentally, as available reports [8,13] deal solely with cases where $\zeta_s < \zeta_r$.

8. Conclusions

In this work, we proposed a minimal model describing the bar-resonator interaction occurring in mallet percussion instruments. The bar is reduced to a single mode, whose motion is described by a disk-shaped oscillator with equivalent modal parameters. The resonator acoustics are described by the acoustic modes of a cylindrical waveguide with closed-open boundary conditions, including radiation damping.

Using 2-D axisymmetric finite element models, we were able to numerically calculate: (1) the effect of the disk presence on the radiation impedance of the pipe and (2) the vibro-acoustic coupling between the disk and the resonator. The numerical results from the FE models were then fitted to simple analytical expressions, that allowed for an approximate description of the three-dimensional coupling effects, adaptable to the simple lumped-parameter modelling framework.

Numerical results from the simplified analytical model were then numerically validated against those from a 2-D vibro-acoustic FE model, yielding similar results, both qualitatively and quantitatively, over a wide range of configurations.

Temporal simulations and an energy balance analysis of the simplified model, demonstrated its capacity to emulate the essential features of the two-way coupling dynamics observed in real instruments. Tuning the disk and resonator frequencies leads to a stronger coupling between the two elements, and increases the radiation efficiency of the system. The model is also able to describe the decrease in decay time of the bar, associated with the large transfers of energy from the bar to the resonator, as reported in previous experimental observations. Additionally, our model suggests that this behavior occurs solely for particular configurations, where the damping of the bar mode is lower than the radiation damping of the resonator $\zeta_s < \zeta_r$, as will be the case for most metallic instruments. For the opposite scenario $\zeta_s > \zeta_r$, our models suggested that the presence of a tuned resonator could increases both the radiation efficiency and the decay time of the system. However, as of yet, no experimental reports are available to validate this behavior.

Contrary to previous work, the simplicity of the proposed model allows for an intuitive comprehension of the coupling dynamics occurring in bar-resonator systems. The proposed model can also be a useful tool in the design and optimization of real instruments, as well as for virtual sound synthesis. Moreover, without significant additional complexity, the general lumped-parameter framework used here can be extended in several directions: (1) including several bar modes and resonator modes, (2) including radiation resistance of the various bar modes, (3) improve the realism of the analytical approximations by fitting coefficients to results from FE models or experiments pertaining to actual bars.

CRediT authorship contribution statement

Filipe Soares: Conceptualization, Methodology, Investigation, Validation, Software, Data curation, Visualization, Writing – original draft, Writing – review & editing. **Jose Antunes:** Investigation, Validation, Supervision, Writing – review & editing. **Vincent Debut:** Supervision, Writing – review & editing.

Data availability

The authors do not have permission to share data.

Declaration of Competing Interest

The authors declare that they have no known competing financial interests or personal relationships that could have appeared to influence the work reported in this paper.

Acknowledgements

The authors gratefully acknowledge the financial support given by "Fundação para a Ciência e Tecnologia" (FCT – Portugal) through the PhD grant referenced SFRH/BD/140598/2018.

References

[1] Henrique L, Antunes J. Optimal design and physical modelling of mallet percussion instruments. Acta Acustica 2003;89:948–63.
[2] Orduña-Bustamante F. Nonuniform beams with harmonically related overtones for use in percussion instruments. J Acoust Soc Am 1991;90 (6):2935–41.
[3] Soares F, Antunes J, Debut V. Multi-modal tuning of vibrating bars with simplified undercuts using an evolutionary optimization algorithm. Appl Acoust 2021;173:107704.
[4] Petrolito J, Legge KA. Optimal undercuts for the tuning of percussive beams. J Acoust Soc Am 1997;102(4):2432–6.
[5] Beaton D, Scavone G. Three-dimensional tuning of idiophone bar modes via finite element analysis. J Acoust Soc Am 2021;149(6):3758–68.
[6] Soares F, Antunes J, Debut V. Tuning of bending and torsional modes of bars used in mallet percussion instruments. J Acoust Soc Am 2021;150(4):2757–69.
[7] Fletcher NH, Rossing TD, editors. The Physics of Musical Instruments. New York, NY: Springer New York; 1998.
[8] Bork I. Practical tuning of xylophone bars and resonators. Appl Acoust 1995;46 (1):103–27.
[9] Henrique L, Inácio O, Paulino J, Antunes J. "Optimization of vibratory and acoustical components of percussion instruments: theoretical and experimental results," in *Forum Acusticum*, Budapest, 2005.
[10] Henrique L, Antunes J, Inácio O, Paulino J. "Application of optimization techniques for acoustical resonators," in *Twelfth International Congress of Sound and Vibration (ICSV12)*, Lisbon, 2005.
[11] Tuttle BC, Burroughs CB. "The effects of a resonator tube on the timbre and directivity of sound radiation from a vibraphone bar," *Proceedings of the Institute of Acoustics - ISMA '97*, vol. 19, no. 5, pp. 207-2011, 1997.
[12] Serra X. "A computer model for bar percussion instruments," in *International Computer Music Conference*. Netherlands: Den Haag; 1986.
[13] Rucz P, Ulveczki MÁ, Angster J, Miklós A. Simulation of mallet percussion instruments by a coupled modal vibroacoustic finite element method. J Acoust Soc Am 2021;149(5):3200–12.
[14] Chaigne A, Doutant V. Numerical simulations of xylophones. I. Time-domain modeling of the vinrating bars. J Acoust Soc Am 1997;101(1):539–57.
[15] Doutant V, Matignon D, Chaigne A. Numerical simulations of xylophones. II. Time-domain modeling of the resonator and the radiated sound pressure. J Acoust Soc Am 1998;104(3):1633–47.
[16] Axisa F, Antunes J. Modelling of Mechanical Systems: Fluid-Structure Interaction. Elsevier Ltd 2007.
[17] Favre JL. Marimba Bar and Resonator Dimensions for La Favre 5-octave instrument [Accessed 2022]. [Online] Available 2007. http://www.lafavre.us/marimba-bars.htm.
[18] Chaigne A, Kergomard J. "Dissipation and Damping," in *Acoustics of Musical Instruments*. New York: Springer-Verlag; 2016. p. 201–3.
[19] Morse P, Ingard K. "Theoretical Acoustics," in *Chapter 7: The Radiation of Sound*. New York: McGraw-Hill Book Company; 1968. p. 389–90.
[20] Olson H. "Acoustical Elements," in *Acoustical Engineering*, New Jersey, D. Van Nostrand Company, Inc., 1957, pp. 92-99.
[21] Mellow T, Karkkainen L. On the sound field of an oscillating disk in a finite open and closed back circular baffle. J Acoust Soc Am 2004;118(3):1311–25.
[22] Levine H, Schwinger J. On the Radiation of Sound from an Unflanged Circular Pipe. Phys Rev 1948;73(4):383–406.
[23] Silva F, Guillemain Ph, Kergomard J, Mallaroni B, Norris AN. Approximation formulae for the acoustic radiation impedance of a cylindrical pipe. J Sound Vib 2009;322(1-2):255–63.
[24] Rucz P, Angster J, Miklós A. "Finite element simulation of radiation impedances with applications for musical instrument design," in *International Symposium on Music Acoustics (ISMA 2019)*. Germany: Detmold; 2019.
[25] Rucz P. A finite element approach for the calculation of the self and mutual radiation impedances of resonators. J Acoust Soc Am 2018;143(4):2449–59.
[26] Lyamshev LM. A question in connection with the principle of reciprocity in acoustics. Soviet Physics Doklady 1959;4:406–9.
[27] ten Wolde T, Verheij JW, Steenhoek HF. Reciprocity method for the measurement of mechano-acoustical transfer functions. J Sound Vib 1975;42 (1):49–55.
[28] T. t. Wolde,. Reciprocity measurements in acoustical and mechano-acoustical systems: Review of theory and applications. Acta Acustica united with Acustica 2010;96:1–13.
[29] Fahy F. The vibro-acoustic reciprocity principle and applications to noise control. Acta Acustica united with Acustica 1995;81(6):544–58.
[30] Fahy F. Some applications of the reciprocity principle in experimental vibro-acoustics. Acoust Phys 2002;49(2):217–29.
[31] Bensoam J, Aussal M. Self and mutual radiation impedances between translated spheroids. Application to parallel disks. J Acoust Soc Am 2021;150 (3):1794–805.
[32] Kinsler L, Frey A, Coppens A, Sanders J. Fundamentals of Acoustics. 4th Edition. New York: John Wiley & Sons Inc; 2000.
[33] Ouisse M, Foltete E. "On the comparison of symmetric and unsymmetric formulations for experimental vibro-acoustic modal analysis," in *Acoustics 08'*, Paris, France, 2008.
[34] Axisa F, Antunes J. "Vibro-Acoustic Coupling," in *Modelling of Mechanical Systems: Fluid-Structure Interaction*, Elsevier Ltd. , 2007, pp. 461-464.

[35] Hambric S, Sung S, Nefske D. Engineering Vibroacoustic Analysis. John Wiley & Sons Ltd 2016.
[36] Wyckaert K, Augusztinovicz F, Sas P. Vibro-acoustical modal analysis: Reciprocity, model symmetry and model validity. J Acoust Soc Am 1996;5 (100):3172–81.
[37] Chaine A, Kergomard J. "Coupled Systems," in *Acoustics of Musical Instruments*, New York, Springer-Verlag, 2016, pp. 282-289.
[38] MATLAB R2021a, [Online]. Available: https://www.mathworks.com/help/matlab/ref/ode23t.html. [Accessed 2021].
[39] Oliveira E, Debut V. Geometry and tuning assessment of timbilas through non-destructive reverse engineering techniques. Acústica 2020 2020.